Clay winnowing associated with wave–current ripple dynamics on cohesive sand–clay beds

X. Wu *University of Hull, Hull, U.K. – x.wu@hull.ac.uk*
J. Malarkey *School of Ocean Sciences, Bangor University, Menai Bridge, U.K. – j.malarkey@bangor.ac.uk*
F. Fernández *Department of Civil and Environmental Engineering, The Pennsylvania State University, State College, USA – roberto@psu.edu*
J. H. Baas *School of Ocean Sciences, Bangor University, Menai Bridge, U.K. – j.baas@bangor.ac.uk*
D. R. Parsons *Loughborough University, Loughborough, U.K. – d.parsons@lboro.ac.uk*

ABSTRACT: A full understanding of ripple dynamics in sand–clay mixtures is essential to improve existing ripple predictors, especially under combined wave–current conditions. We conducted a series of experiments in a large recirculating flume, with initial clay contents, C_0, ranging from 0 to 18.3%, in the Total Environment Simulator at the University of Hull. The experimental results reveal that winnowing-induced clay loss from beds is associated with two distinct types of equilibrium combined-flow ripples, separated by a discontinuity at C_0 = 10.6%: large clean-sand ripples and small, flat ripples. Most importantly, for the first time, we combine earlier experimental results to quantify the influence of both clay and hydrodynamic forcing on ripple morphology. Additionally, the present experiments show the difference in clay winnowing efficiency over flat and rippled beds under different flow conditions and will prove beneficial in stimulating further research focusing on the factors controlling the clay winnowing process.

1 INTRODUCTION

Flume studies concerning ripple dynamics on beds of well-sorted clean sand under different flow conditions (e.g., Pedocchi and García, 2009, Perillo et al., 2014) have provided high-quality process information for developing empirical formulae to predict ripple dimensions. However, the existing ripple predictors are of limited use for the majority of estuarine and coastal environments, where sediment almost universally consists of mixtures of cohesive clay and non-cohesive sand. More recently, researchers have therefore focused on ripple dynamics within substrates composed of mixtures of sand and clay under currents and waves (Baas et al., 2013, Wu et al., 2018). Moreover, Wu et al., (2022) studied the influence of clay on ripple development under combined wave-current flows and highlighted the significant decrease in ripple dimensions with an initial clay content, C_0, greater than 10.6%. While these studies have identified the role clay winnowing from the bed has played in ripple development, it is still unclear which factors control clay winnowing efficiency. Therefore, the present study extends Wu et al.'s (2022) research, with further experiments under a wider range of hydrodynamic conditions. The specific objectives were: (1) to compare ripple development on beds with similar clay content under different hydrodynamic conditions; (2) to compare clay winnowing efficiency, based on quantifying bed clay content during ripple development, under different types of flow conditions.

2 METHODS

2.1.1 Experiment setup

The experiments were undertaken in a recirculating flume tank, the Total Environment Simulator at the University of Hull. Three equal channels, 11 m long and 1.6 m wide, were separated by brick walls, 0.2 m high, in the tank (Figure 1). Combined flow conditions were maintained during the

experiments and flow velocities in each channel were measured by a 25 Hz Vectrino profiler. Freshwater was used in all experiments, with a water depth of 0.4 m. A 2-MHz ultrasonic ranging sensor (URS), containing 32 probes, monitored the bedform evolution in the test section (Figure 1).

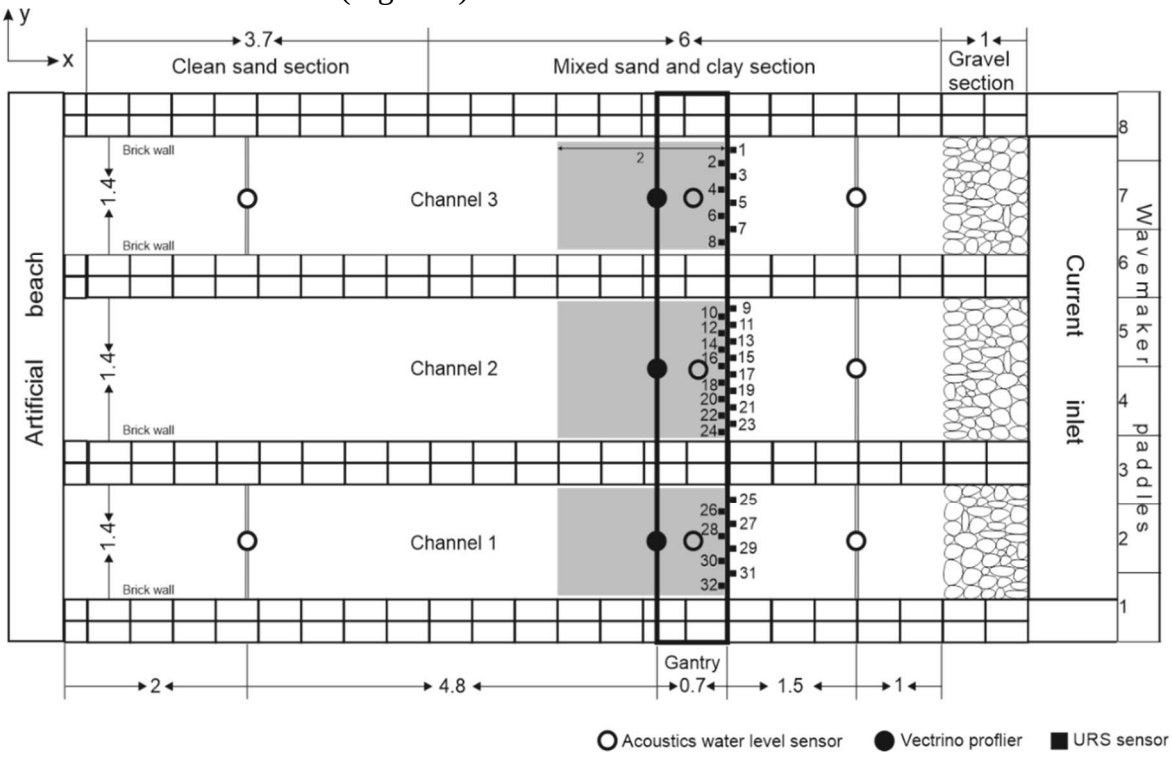

Figure 1. Plan view of the experimental setup. The grey area was scanned by an Ultrasonic Range System (URS) with numbered sensors (black squares). White and black circles denote acoustic water level sensors and Vectrino profilers, respectively. Dimensions are in metres.

2.2 Experimental procedure

Wu et al.'s (2022) wave-dominated flow condition (WC1), with a depth-average current, U_c ~ 0.16 m s^{-1}, and wave velocity amplitude, U_o ~ 0.32 m s^{-1}, was added to in this paper with two further flow conditions (WC2 and WC3) with U_c ~ 0.3 m s^{-1} and U_o ~ 0.27 and 0.13 m s^{-1} (Table 1). The flow conditions are numbered according to increasing relative current strength from WC1-WC3. The experiments involved different mass concentrations of initial clay, C_0, in each of the three channels, with the same flow conditions for each channel. The bed was composed of a well-sorted sand with a median diameter, D_{50}, of 0.45 mm and cohesive kaolinite clay with D_{50} = 0.089 mm. The order of the experiments was from high to low clay content, by taking advantage of the natural winnowing of the bed during the experiment.

To ensure homogeneity in the mixed section of each channel (Figure 1), the clay was mixed into the sand using a handheld mixer and levelled between runs. A terrestrial 3D laser scanner was used to scan the sediment bed in each channel before and after the run, without water in the tank. Ripple development was recorded using an Ultrasonic Range System (URS) and pre- and post-experiment sediment cores were collected from the bed using syringes with a diameter of 20 mm and a maximum length of 90 mm. Channel 1 of Run A2 and Channel 2 of Run B4 were excluded from the analysis, because the sediment in these channels was not sufficiently well mixed.

2.3 Data processing

Raw bed elevation profiles (BEPs) recorded from each URS scan, were analysed using a standard 'peaks and troughs' procedure to identify individual ripple heights, η, and wavelengths, λ, and their mean values, λ_t and η_t, at time, t, to construct

the development curves of ripple dimensions and determine

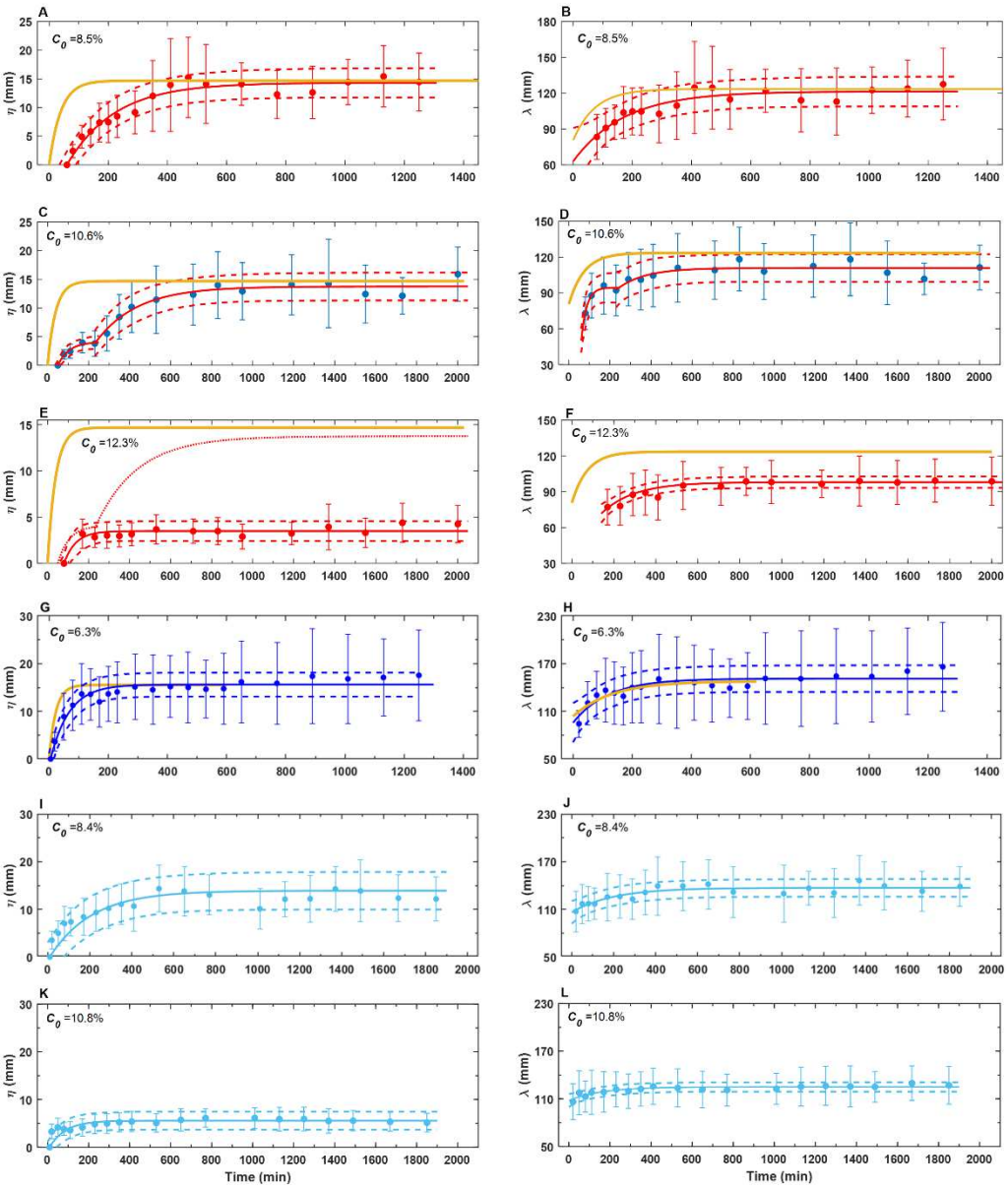

Figure 2. Development of ripple height and wavelength for WC1 (red dots in A - F) (Wu et al., 2022), WC3 (dark blue dots in G – H) and WC2 (light blue dots in I - L) for different values of C_0. The vertical lines denote one standard deviation from the mean dimension. Red, dark and light blue lines are based on fitting to Equations 1 and 2, and dashed lines are their corresponding 95% confidence intervals. The yellow lines are best-fit curves for the clean-sand counterparts, under WC1 and WC3 conditions.

equilibrium bedform dimensions, following Wu et al.'s (2022) procedure:

$$\frac{\eta_t}{\eta_e} = 1 - 0.1^{\frac{t-t_i}{T_\eta - t_i}}, \quad (1)$$

$$\frac{\lambda_t - \lambda_i}{\lambda_e - \lambda_i} = 1 - 0.1^{\frac{t-t_i}{T_\lambda - t_i}}, \quad (2)$$

where η_e and λ_e, are the equilibrium height and wavelength, T_η and T_λ are the equilibrium time for the height and wavelength, t_i is the initiation time and λ_i is the initial wavelength. The ripples were also characterised by their steepness (RS) = η_e/λ_e, and ripple symmetry index (RSI) = λ_s/λ_l, where λ_s and λ_l are the length of the stoss and lee side of the ripple (RSI < 1.3 for symmetric and 1.3 < RSI < 1.5 for quasi-asymmetric ripples, Perillio et al., 2014) (Table 1).

Table 1 Experimental parameters and bedform characteristics

Run /Channel	Flow code[1]	Duration (min)	C_0 (%)	U_o (m s^{-1})	U_c (m s^{-1})	η_e (mm)	T_η (mm)	λ_e (mm)	T_λ (mm)	RSI	RS	Plan view
A1/2	WC1	1970	0	0.32	0.16	14.4	90	123.6	170	1.4	0.12	2D
A3/1	WC1	1250	5.7	0.32	0.19	14.7	125	126.5	330	1.4	0.12	2D
A3/2	WC1	1250	8.5	0.31	0.16	14.3	432	121.4	456	1.4	0.11	2D
A2/2	WC1	1250	10.6	0.33	0.19	13.7	678	110.9	540	1.3	0.14	2D
A3/3	WC1	2000	11.6	0.31	0.15	4.1	271	108.5	382	1.5	0.05	3D
A2/3	WC1	2000	12.3	0.33	0.2	3.5	211	98	499	1.5	0.04	3D
B1/2	WC3	600	0	0.14	0.31	15.5	53	147.9	302	1.5	0.11	2D
B4/1	WC3	1250	2.5	0.13	0.25	14.8	71	144.8	330	1.5	0.11	2D
B4/3	WC3	1250	6.4	0.12	0.29	15.6	151	152	342	1.5	0.1	2D
B2/1	WC3	650	9.9	0.13	0.31	-	-	-	-	-	-	-
B2/2	WC3	650	13.1	0.14	0.29	-	-	-	-	-	-	-
B2/3	WC3	650	18.3	0.13	0.31	-	-	-	-	-	-	-
B3/1	WC2	1850	8.4	0.27	0.32	13.9	471	137	465	1.4	0.09	2D
B3/2	WC2	1850	10.8	0.27	0.3	5.6	273	125	377	1.6	0.04	3D
B3/3	WC2	1850	16.3	0.27	0.31	-	-	-	-	-	-	-

[1]Flow code number signifies increasing relative current strength compared to WC1.

Sediment cores from the initial flat bed and the ripple crests and troughs were sliced into 5- and 10-mm intervals for grain size analysis using a Malvern Mastersizer 2000. Crest and trough cores were combined to form one continuous profile through the active layer (ripple crest down to trough) and into the substrate beneath. The measured clay content, C, in the sediment cores was further processed to acquire the total amount of clay removed from the bed, I, by integrating the clay deficit, defined as $C_{def} = C_0 - C$, from the lowest reference level, $z = -b$ up to the crest level, $z = 0$.

3 RESULTS

3.1 Ripple development

Under WC1 conditions, increasing C_0 slowed ripple development compared to the clean-sand case (Figure 2A-D). This is particularly true for C_0 = 10.6%. Ripples experienced two stages of development; the ripple height and wavelength only grew to 3.9 and 96.2 mm at t = 170 min, thereafter, the ripples experienced a period of relatively rapid, yet gradually decelerating, growth in the next approximately 7 hours, reaching η_e = 13.7 mm and λ_e = 110.9 mm with 2D plan view geometry (Figure 2C – D, Table 1). For C_0 = 12.3%, the initial ripple height growth trend was similar to its 10.6% counterpart until t = 230 min. However, thereafter, the ripples experienced weak growth in the remainder of the experiment. The equilibrium ripples were asymmetric and 3D, with η_e = 3.5 mm and λ_e = 98 mm (Table 1).

For C_0 = 6.4% under WC3 conditions, the ripples developed to similar equilibrium dimensions as their clean-sand counterparts, η_e = 15.6 mm and λ_e = 152.5 mm (Figure 2C, D), and the bed was again covered in 2D, quasi-asymmetric ripples (Table 1).

For C_0 = 8.4% under WC2 conditions, ripple dimensions experienced a gradual development period of around seven hours before reaching stability, with η_e of 7.1 and λ_e of 110.8 mm (Figure 2I and J). Equilibrium ripples retained similar geometries to those developed under WC3 conditions, characterised by 2D plan forms and quasi-asymmetric cross sections (Table 1).

For C_0 = 10.8% (WC2), the ripple height was 3.3 mm at t = 20 min, followed by a period of slow growth up to η_e = 5.6 mm at t = 230 min, beyond which the ripple height grew no further (Figure 2K). The small ripples formed were 3D with discontinuous, sinuous crestlines in plan view. In cross-section, these ripples were slightly asymmetric and of limited steepness, with RSI = 1.6 and RS = 0.04 (Table 1).

3.2 Comparison of pre- and post-experiment vertical bed clay content

Under WC1 conditions, for C_0 = 10.6%, at the end of the experiment, the sediment cores reveal 100% clay loss in the active layer (ripple crest down to the ripple trough); there was a layer, with thickness of ~ 60 mm of reduced clay, beneath the ripple base (Figure 3A). The equivalent clean-sand depth (black horizontal dashed line), $d_c = I/C_0$, was 43 mm. Compared to the ripple height, d_c gives an indication of how much clean sand is available for ripples to grow (Wu et al., 2022). Small ripples, for the C_0 = 12.3% case, retained 8% clay near the base, with a thin layer of reduced clay content beneath the ripple base (Figure 3B).

Similarly, under WC3 condition, for C_0 = 6.4%, the clay content in the active layer of the ripples was zero and a layer of reduced clay content extended down to c. 80 mm by the end of the experiment (dark blue symbols and lines in Figure 3C), with d_c = 57 mm, more than two times the ripple height.

In the C_0 = 8.4% (WC2) case, a small amount of clay, approximately 2.8%, remained at the base of the ripples at the end of the experiment (Figure 3E). Compared to the C_0 = 8.4% case, the base of the small ripples, for C_0 = 10.8%, contained a higher amount of clay (9.8%) and d_c = 10.1 mm (Figure 3F).

No ripples formed for $C_0 \geq$ 9.9% under WC3 conditions and C_0 = 16.3% under WC2 conditions (Table 1). Sediment cores collected from the flat beds after these experiments show vertically-constant clay loss from the entire bed (Figure 3D, G). On beds with C_0 = 16.3% and 18.3%, there was an approximate 10% reduction in clay content and d_c was approximately 17 mm and 15 mm, respectively.

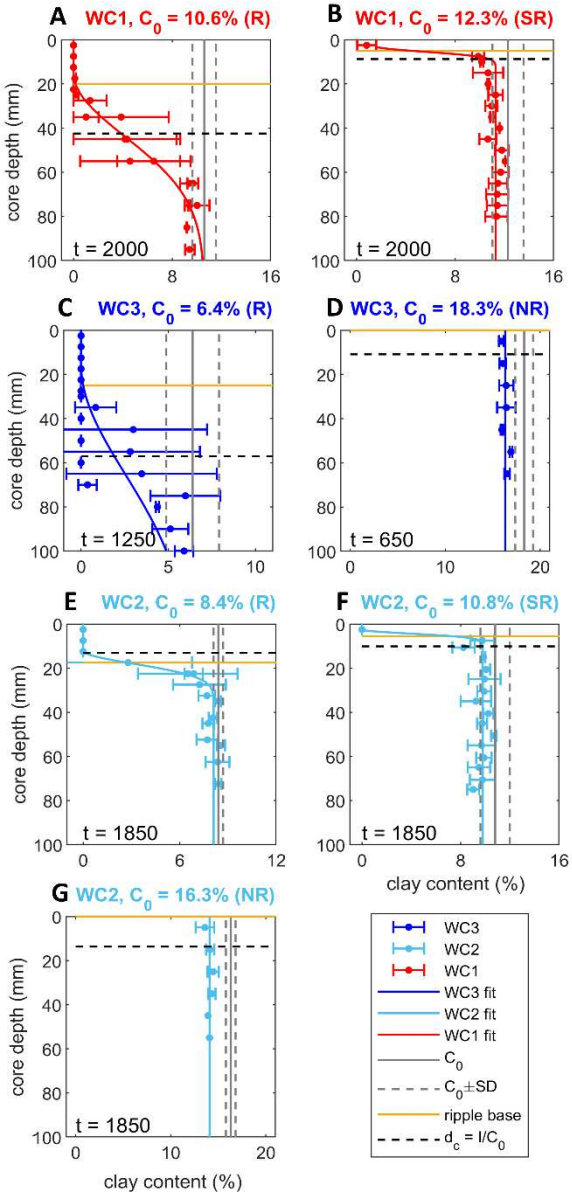

Figure 3. Vertical profiles of clay content in cores collected from beds in the mixed sand-clay section post experiment under WC1 conditions (A - B), WC3 conditions (C - D), and under WC2 conditions (E - G). The red, dark and light blue solid lines are the fits to WC1/WC3/WC2 clay content at each depth. The grey vertical solid and dashed lines represent mean initial clay content and one standard deviation from the mean. The horizontal bars denote one standard deviation of the mean clay content at that depth. The yellow lines represent the ripple base. The dashed horizontal black line is the equivalent clean-sand depth.

4 DISCUSSION

4.1 The effect of clay and hydrodynamic conditions on ripple dimensions

The ripple steepness and wavelength for all cases are listed in Table 1; there are two quite distinct constant steepness groupings, η_e/λ_e, related to the large and small ripples with a change at $C_0 = 10.6\%$. For large ripples the steepness decreases with increasing current strength: $\eta_e/\lambda_e \sim 0.12$, for $U_c \sim 0.16$ m s^{-1}, WC1; and 0.103, for $U_c \sim 0.3$ m s^{-1}, WC2 and WC3 (Tables 1). This is the current shearing the tops off the ripple crests with increasing effect, such that for the strongest current the steepness is only just above the threshold for oscillatory boundary-layer separation ($\eta_e/\lambda_e > 0.1$). The small ripples have a steepness of ~ 0.04. While there is a sudden change in ripple steepness and height, there is a gradual decrease in wavelength with increasing C_0, for $C_0 \geq 8.5\%$.

4.2 Quantifying the clay loss

Significant clay loss beneath equilibrium ripples was observed on beds with $C_0 \leq 10.6\%$ (Figure 3A, C). However, such deep cleaning of the bed clay was considerably weakened in the $C_0 = 8.4\%$ (WC2) case, despite the increased hydrodynamic forcing (Figure 3E).

We quantified the clay loss under different flow conditions by calculating the mass flux of clay out of the bed, $F_b = I/t_d$, where t_d, is the experiment duration. For large ripples this gives $F_b \sim 3.5\times10^{-6}$ g mm^{-2}min^{-1}, under WC1 and WC3 conditions, compared to 9.4×10^{-7} g mm^{-2}min^{-1} under WC2 conditions. This latter value is comparable to that being removed from small-rippled beds in the WC1 and WC2 cases, with $F_b \sim 8.5\times10^{-7}$ g mm^{-2}min^{-1}. This difference in deep cleaning between WC2 and WC3 is also seen in the cases where no ripples formed, even though the fluxes are two orders of magnitude smaller: $F_b \sim 5\times10^{-8}$ g mm^{-2}min^{-1} for WC3 and $F_b = 2\times10^{-8}$ g mm^{-2}min^{-1} for WC2.

5 CONCLUSIONS

The following conclusions are drawn:

1. The experimental results reveal that two distinct types of equilibrium ripples develop. For $C_0 \leq 10.6\%$, large 2D, quasi asymmetric equilibrium ripples develop, with dimensions similar to their clean-sand counterparts; for $C_0 > 10.6\%$, small, flat, and more asymmetric equilibrium ripples develop.
2. There were two quite distinct constant steepness groupings associated with this change at $C_0 = 10.6\%$, with a value 0.04 for the small ripples. For larger ripples, the steepness decreased with increasing current strength. The ripple wavelength decreases for $C_0 > 8.5\%$.
3. Winnowing-induced deep cleaning of bed clay under large ripples occurred under WC1 and WC3 conditions, but was inhibited under WC2 conditions, which is reflected in a reduction of the clay flux out of the bed by a factor of four.

6 ACKNOWLEDGEMENT

We acknowledge funding by the European Research Council under the European Union's Horizon 2020 research and innovation program (grant no. 725955). Participation of R. Fernández was also supported by the Leverhulme Trust and Leverhulme Early Career Researcher Fellowship (grant ECF-2020-679).

7 REFERENCES

Baas, J. H., Davies, A. G. & Malarkey, J. 2013. Bedform development in mixed sand–mud: The contrasting role of cohesive forces in flow and bed. Geomorphology, 182, 19-32.

Pedocchi, F. & García, M. 2009. Ripple morphology under oscillatory flow: 2. Experiments. Journal of Geophysical Research: Oceans, 114.

Perillo, M. M., Best, J. L. & Garcia, M. H. 2014. A new phase diagram for combined-flow bedforms. Journal of Sedimentary Research, 84, 301-313.

Soulsby, R. (1997). Dynamics of marine sands: A manual for practical applications. Thomas Telford.

Wu, X., Baas, J. H., Parsons, D. R., Eggenhuisen, J., Amoudry, L., Cartigny, M., Mclelland, S., Mouazé, D. & Ruessink, G. 2018. Wave Ripple Development on Mixed Clay - Sand Substrates: Effects of Clay Winnowing and Armoring. Journal

of Geophysical Research: Earth Surface, 123, 2784-2801.

Wu, X., Fernández, R., Baas, J.H., Malarkey, J. & Parsons, D.R. 2022. Discontinuity in equilibrium wave-current ripple size and shape and deep cleaning associated with cohesive sand-clay beds. Journal of Geophysical Research Earth Surface, 127, e2022JF006771.